Construction of a high-resolution DEM of an Arctic ice cap using shape-from-shading

A. W. BINGHAM[†] and W. G. REES[‡]

[†] Jet Propulsion Laboratory, California Institute of Technology, 4800 Oak Grove Drive, Pasadena, CA 91109, U.S.A.

[‡] Scott Polar Research Institute, University of Cambridge, Lensfield Road, Cambridge, CB2 1ER, U.K.

Tel: +1 818 354 1940 Fax: +1 818 393 6720 email: awb@pacific.jpl.nasa.gov

Abstract. Digital elevation models (DEMs) of ice sheets and ice caps are usually constructed from elevation data acquired from airborne or satellite-borne altimetric systems. Consequently, the DEMs have a spatial resolution of about 1 km which limits their use for most glaciological and remote sensing studies. In this paper we investigated the possibility of using a shape-from-shading technique, applied to a Landsat MSS image, to create a high spatial resolution DEM of Austfonna, an ice cap in Svalbard. A high correlation (coefficient of determination = 0.85) was observed between Landsat pixel brightness values, acquired during winter, and the surface slope component parallel to the solar azimuth. This relationship was used to create a DEM by calculating surface elevation profiles across the ice cap, using low spatial resolution radio echo sounding data as tie points. The resulting DEM had an estimated RMS error of about 14 m, with the error occurring mostly at low spatial frequencies. Shape-from-shading produces less accurate DEMs than interferometric SAR

(InSAR) techniques. Nevertheless, in scenarios for which InSAR can not be used to construct a DEM, shape-from-shading provides an acceptable alternative.

SHORT TITLE: DEM derived by shape-from-shading

1. Introduction

Surface topography is a primary data source for most glaciological and remote sensing studies of terrestrial polar ice masses (glaciers, ice caps and ice sheets). Surface morphology is used to delineate drainage basins, study ice rheology and analyse the spatial distribution of surface features (e.g. Drewry 1983, Dowdeswell 1986). Information on surface topography is also required to model processes such as heat budget for climatological studies, ice dynamics and mass balance (e.g. Huybrechts *et al.* 1991, Arnold *et al.* 1996). Remotely sensed imagery acquired from side-looking sensors are distorted by terrain effects. High spatial resolution digital elevation models (DEMs) are needed to correct for this distortion and also to permit accurate geocoding (Johnsen *et al.* 1995). DEMs provide detailed information about local slope and this is used to extract geophysical parameters from remotely sensed data (e.g. Dozier and Warren 1982).

At the spatial scale of a glacier (area $< 10^2$ km^2), stereographic aerial photography is used to construct high spatial resolution DEMs. For example, Fox and Nuttall (1997) have presented a DEM of Finsterwalderbreen, Svalbard, with a grid spacing of 25 m. At coarser spatial scales, DEMs are constructed using altimetric data. Satellite stereographic methods, using SPOT or RADARSAT image pairs, are not an option at these scales because the featureless terrain makes it difficult to match pairs of imagery. For ice caps (10^2 km^2 < area < 10^5 km^2) airborne radio echo sounding (RES) techniques are normally used to construct DEMs (e.g. Dowdeswell *et al.* 1984), and for ice sheets (area > 10^5 km^2) satellite altimetry is used (e.g. Zwally *et al.* 1983, Bamber 1994). However, DEMs derived from altimetric data typically have a grid spacing greater than 1 km which limits their application. The aim of this paper was to create a high spatial resolution DEM of Austfonna, an ice cap in the High Arctic. A shape-from-shading technique was applied to visible Landsat MSS imagery

to construct high spatial resolution profiles of the surface. These profiles were constrained by low spatial frequency RES elevation data to produce a new DEM.

2. Study area and data set

Austfonna is an ice cap on the island of Nordaustlandet, north-east Svalbard (figure 1). It extends over an area of 8100 km^2 and is one of the largest ice caps in the Northern Hemisphere. In spring 1983 the Scott Polar Research Institute (SPRI) determined the surface and bedrock elevation of Austfonna using airborne RES methods (Dowdeswell *et al.* 1986). These data were collected at spatial intervals of about 100 m along flight lines on a 15 km grid (figure 2) and used here to create an initial low spatial resolution DEM in order to constrain the high spatial resolution DEM.

Two cloud-free Landsat/MSS images of Nordaustlandet were analysed in this study, one acquired in winter 1973 and the other in summer 1981 (figure 3). Both images were radiometrically corrected, georeferenced to UTM zone 35 map coordinates using ground control points determined from a topographic map of Nordaustlandet (Dowdeswell 1984), and resampled to a spatial resolution of 100 m.

3. Gridding strategies

DEMs are constructed by gridding irregularly spaced surface elevation data onto a regularly spaced lattice. This involves estimating the surface elevation at each grid point, based on a function derived from values observed at arbitrary locations. Initially, we constructed a DEM of Austfonna by gridding the RES surface elevation using a minimal squared curvature function (Smith and Wessel 1990), but the grid spacing of the derived DEM was limited by the spatial density of the RES data. It is estimated, based on the geometric mean of the along and across-track resolutions, that the

minimum reasonable grid spacing of the DEM is 1 km. In theory, it is possible to improve the spatial resolution of this DEM by merging the RES data with an alternative data set that contains topographic information. Two merging techniques that can be used are interferometric SAR (InSAR) and shape-from-shading.

3.1. *Interferometric SAR*

The application of InSAR for producing DEMs of terrestrial ice masses has been the focus of considerable recent research (e.g. Kwok and Fahnestock 1996, Joughin *et al.* 1996). Joughin (1995) has shown that InSAR-derived DEMs, created using a method of double-differencing, have relative errors approaching 2 m. More recently, Unwin and Wingham (1997) have used these techniques combined with RES data to create a DEM of the central part of Austfonna that has an accuracy of about 8 m. Although InSAR is extremely promising, currently it is not practical for constructing DEMs of large Arctic ice masses. The technique requires several highly correlated SAR images but these are often difficult to acquire because backscatter is affected by weather-induced changes in the surface conditions. In addition, streak-noise in interferograms of ice sheets limits the accuracy of the derived DEMs (Joughin 1995).

3.2. *Shape-from-shading*

Shape-from-shading exploits the relationship between surface slope and brightness (in optical imagery) or backscatter (in radar imagery) to extract surface topography. Previous studies have noted that remotely sensed optical imagery of terrain covered with snow and ice contains topographic information (Dowdeswell and McIntyre 1987, Stephenson and Zwally 1989), and Rees and Dowdeswell (1988) demonstrated a linear relationship between Landsat MSS brightness values and

local slope. Cooper (1994) exploited this relationship by devising a shape-from-shading algorithm to produce a topographic map from a SPOT image, but the algorithm lacked tie points and the accuracy of the map was not demonstrated. Fiksel *et al.* (1994) applied shape-from-shading to SAR imagery over Antarctica, but their techniques are not transferable to the Arctic because the effects of melting obscure topographic signals in SAR backscatter images.

Most shape-from-shading algorithms assume that a surface has Lambertian scattering properties. Therefore, the image brightness (pixel value) is described by the general equation (Cooper 1994):

$$I(x,y) = \frac{\alpha\frac{\partial z}{\partial x} + \beta\frac{\partial z}{\partial y} + \gamma}{\left(1 + \left(\frac{\partial z}{\partial x}\right)^2 + \left(\frac{\partial z}{\partial y}\right)^2\right)^{1/2}} I_0, \quad (1)$$

where α, β and γ are the Cartesian components of the unit vector in the direction of solar illumination; x, y and z are Cartesian coordinates of the surface with x and y in the horizontal plane and z vertical; I_0 is the image brightness for a normally-illuminated pixel.

Two simplifications are made to equation 1. The first is to assume that slopes are small, such that:

$$\left(\frac{\partial z}{\partial x}\right)^2 + \left(\frac{\partial z}{\partial y}\right)^2 \approx 1 \quad (2)$$

For polar ice caps where surface slopes are typically less than 3°, this assumption holds. The second simplification is to choose a Cartesian coordinate system in which x is aligned to the solar azimuth, such that $\beta = 0$. This change in the coordinate system and substitution of equation 2 into equation 1 gives:

$$I(x) = \alpha'\frac{\partial z}{\partial x} + \gamma', \quad (3)$$

where $\alpha' = \alpha I_0$ and $\gamma' = \gamma I_0$.

This equation was validated for Austfonna by plotting surface slopes along transects parallel to the solar azimuth against Landsat MSS pixel brightness values. The slopes are calculated using the DEM derived from RES data, gridded using a minimum curvature algorithm. Figure 4 shows that there is a high correlation ($r^2 = 0.84$) between surface slope and brightness values in the winter, but no correlation in the summer. The straight line equation that best fits the winter Landsat data is given by: $I(x) = 1.728\ \partial z/\partial x + 17.24$. For large negative slopes the data deviate from the straight line. This is because the transect passes across a drainage basin that has undergone past surge activity (Dowdeswell and McIntyre 1987) resulting in large scale (3-4 km) surface roughness patterns that are not resolved by the DEM. The calculated RMS uncertainty in the surface slope is 0.82° which represents the intrinsic accuracy of the shape-from-shading technique when applied to winter Landsat MSS imagery. This uncertainty is caused by variations in the bi-directional reflectance distribution function (BRDF) resulting from variations in the snow surface properties, such as grain size and surface roughness (e.g. sastrugi and crevasses).

4. Method

4.1. *Implementation of shape-from-shading*

Surface elevation, z, along a transect parallel to the solar azimuth is obtained by integrating equation 3:

$$z(x) = \frac{1}{\alpha'}\int_o^x I(x)dx - \frac{\gamma' x}{\alpha'} + C, \qquad (4)$$

where x is along-transect distance and C is the constant of integration. In discrete form, this is written as:

$$z(i) = a\sum_{n=0}^{i} I(n) + bi + c, \quad (5)$$

where $a = p/\alpha'$, $b = -\gamma' p/\alpha'$, $c = C$ and $i = xp$; p is the distance between pixels. Alternatively, this may be expressed in matrix notation as:

$$\mathbf{z} = \mathbf{A} \cdot \mathbf{x} \quad (6)$$

where $\mathbf{z}$ is a vector of surface elevation tie points, $\mathbf{A}$ is a matrix of the sum of brightness values and pixel distance along-transect, and $\mathbf{x}$ is a vector of coefficients. If surface elevation is known for at least three positions, equation 6 can be solved using standard numerical techniques (e.g. Press et al. 1992) and subsequently used to evaluate surface elevation at every point along a transect. For example, if surface elevation, z, is known at three positions i = 1, 2 and 3 along-transect, the parameters in equation 6 can be expressed as:

$$\mathbf{z} = \begin{pmatrix} z(i_1) \\ z(i_2) \\ z(i_3) \end{pmatrix}, \quad \mathbf{A} = \begin{pmatrix} \sum_{n=0}^{i_1} I(n) & i_1 & 1 \\ \sum_{n=0}^{i_2} I(n) & i_2 & 1 \\ \sum_{n=0}^{i_3} I(n) & i_3 & 1 \end{pmatrix}, \quad \mathbf{x} = \begin{pmatrix} p/\alpha' \\ -\gamma' p/\alpha' \\ c \end{pmatrix}.$$

Several algorithms were tested for calculating along-transect elevation and it was concluded that a piecewise algorithm is most accurate. The algorithm we choose to adopt is as follows:

- solve **x** (equation 6) using the first three tie points along a transect,
- calculate surface elevation between the start of the transect and the second tie point,
- solve **x** using the second, third and fourth tie points,
- calculate elevation between the second and third tie points,
- repeat the process until the end of the transect is reached.

A drawback of using just three tie points at a time is that the set of equations, described by equation 6, can become close to singular. To minimise this effect, we have solved the equations using the method of singular value decomposition. Nevertheless, the effect of singularity can occasionally cause discontinuities at tie-points, resulting in large deviations (> 30 m) as illustrated in figure 5. Although the use of more than three tie points would reduce this problem, the solution to **x** would be less representative of the local slope; for this reason we opted to use three tie and acknowledge that large errors can occasionally result.

4.2. *Construction of the DEM*

A new high spatial resolution DEM of Austfonna is constructed by using shape-from-shading applied to a winter Landsat MSS constrained with RES surface elevation data. To achieve this, a total of 2000 brightness value profiles were extracted from the band 4 winter Landsat MSS image. Each profile was along a transect running parallel to the solar azimuth, and the profiles were separated by one pixel (100 m) in the east-west direction. At each crossover between a transect and RES flight line, the interpolated RES surface elevation and the distance along transect were recorded and used to construct matrix **A** (equation 6). These crossovers were used as tie points to determine along-transect elevations, as outlined in the previous section. In this way, surface elevation was calculated at every pixel within the Landsat MSS image and used to produce a DEM with a grid spacing of 100 m.

5. Results

Figure 6 shows the DEM of Austfonna derived from shape-from-shading of a Landsat MSS image constrained with RES surface elevation data. Comparison with Dowdeswell's original topographic

map (Dowdeswell 1984) illustrates no major problems with this gridding method. The summits of Austfonna and Sørfonna are easily identifiable in the DEM and the shapes of the contours are similar to those on the topographic map.

Error in the DEM is evaluated by calculating the difference between the RES tie points and the corresponding heights in the DEM (determined with a bilinear interpolator). A RMS error of 13.6 m is calculated for a total of 18594 tie points. This error is associated with the algorithm used to constrain the shape-from-shading derived elevations with the RES data. Calculation of the Fourier transform of the errors for 512 RES tie points along a 66 km flight line (figure 7) shows that the error mostly occurs at spatial frequencies of less than 1.5 km^{-1} ($\lambda > 670$ m).

The accuracy of the DEM was checked further by calculating semivariograms for linear transects of the surface. Previous analyses of the surface of Nordaustlandet (Rees 1992, 1995) have shown that for spatial scales δ between 100 m and 10 km, the surface is characterised by a semivariance γ that is given by:

$$\gamma \propto \delta^m.$$

The constant m is typically between 1.6 and 1.8. However, for a DEM derived by linear or bilinear interpolation the value of m would tend to 2 for small values of δ. Analysis of the DEM described in this paper gives values of m lying between 1.69 ± 0.04 and 1.83 ± 0.04, depending on the orientation of the transect. These values of m are consistent with previous analyses and are significantly different from the results of linear or bilinear interpolation. The values of γ, calculated for a scale of 1 km, are between 90 and 160 m^2, again depending on the orientation of the transect. These values are consistent with the value of 100 m^2 estimated from the data presented by Rees (1992, 1995).

6. Conclusions

In this paper a shape-from-shading algorithm, constrained with RES elevation data, has been used to construct a high spatial resolution DEM of Austfonna. We have shown that pixel brightness values in a winter visible satellite image have a high correlation with surface slopes ($r^2 = 0.85$). Moreover, a simple shape-from-shading model applied to visible satellite imagery may be used to estimate local surface slope to an accuracy of $\pm 0.8°$ and this is implemented to create a new high spatial resolution DEM of Austfonna. The estimated RMS error in the DEM is 13.6 m and potentially a fine grid spacing, depending on the satellite sensor, can be achieved. This error results from the algorithm used to solve the equations for along-transect surface elevation. Implementation of the shape-from-shading technique would therefore benefit from the use of a more sophisticated inversion algorithm. A further refinement to the technique would involve use of a second winter visible image acquired at a different time of day. Two images with different solar azimuths provide different surface slope information and could potentially improve the detail of the DEM.

Using InSAR techniques to derive a DEM of the central part of Austfonna, Unwin and Wingham (1997) have shown that it is possible to create a DEM with an RMS error of 8 m and a spatial resolution of 40 m. Other work (e.g. Joughin 1995) has shown that InSAR is capable of accuracies of 2 m. Clearly, InSAR is a superior technique to shape-from-shading for constructing DEMs of Arctic ice caps and ice sheets. With the availability of ERS-1/ERS-2 tandom mission and Radarsat SAR imagery, ERS-1/ERS-2 radar altimetric data and proposed future laser altimetric data, it is likely that the production of ice cap and ice sheet DEMs is best achieved using InSAR. However, when this technique fails to perform, either because there is no available imagery or unacceptable streak noise, shape-from-shading provides a potential alternative.

Acknowledgements

This research was funded through a Natural Environment Research Council PhD studentship and National Research Council – JPL research fellowship. The authors are grateful to Prof. Julian Dowdeswell and Dr. Martin Siegert, University of Bristol, for supplying RES and Landsat MSS data. Thanks are due also to Dr. Graham Robertson, University of Oxford, for useful discussions concerning linear equations, Dr. Gareth Marshall, British Antarctic Survey, who provided the map of Svalbard and Marty Marra of Vexcel Corporation.

References

ARNOLD, N.S., WILLIS, I.C., SHARP, M.J., RICHARDS, K.S., and LAWSON, W.J., 1996, A distributed surface energy-balance model for a small valley glacier. I. Development and testing for Haut Glacier dArolla, Valais, Switerland. *Journal of Glaciology*, **42**, 77-89.

BAMBER, J.L, 1994, A digital elevation model of the Antarctic ice sheet derived from ERS-1 altimeter data and comparison with terrestrial measurements. *Annals of Glaciology*, **20**, 48-54.

COOPER, A.P.R., 1994, A simple shape-from-shading algorithm applied to images of ice-covered terrain. *I.E.E.E. Transactions on Geoscience and Remote Sensing*, **32**, 1196-1198.

DOWDESWELL, J.A., 1984, *Remote sensing studies of Svalbard glaciers*, Ph.D. thesis, Scott Polar Research Institute, University of Cambridge.

DOWDESWELL, J.A., 1986, Drainage-basin characteristics of Nordaustlandet ice caps, Svalbard. *Journal of Glaciology*, **32**, 31-38.

DOWDESWELL, J.A., DREWRY, D.J., COOPER, A.P.R., GORMAN, M.R., LIESTØL, O., and ORHEIM, O., 1986, Digital mapping of the Nordaustlandet ice caps from airborne geophysical investigations. *Annals of Glaciology*, **8**, 51-58.

DOWDESWELL, J.A., and MCINTYRE, N.F., 1987, The surface topography of large ice masses from Landsat imagery. *Journal of Glaciology*, **33**, 16-23.

DOZIER, J., and WARREN, S.G, 1982, Effect of viewing angle on the infrared brightness temperature of snow. *Water Resources Research*, **18**, 1424-1434.

DREWRY, D.J., 1983, *Antarctica: glaciology and geophysical folio* (Cambridge: Scott Polar Research Institute, University of Cambridge).

FIKSEL, T., HARTMANN, R., and WINZER, W., 1994, ERS-1 data for mapping of the Antarctic Peninsula by shape-from-shading technique. *Space at the service of our environment, Proceedings of the Second ERS-1 symposium held in Hamburg, Germany, on 11-14 October 1993*, SP-361 (Paris: European Space Agency), pp. 153-158.

FOX, A.J., and NUTTALL, A-M., 1997, Photogrammetry as a research tool for glaciology. *Photogrammetric Record*, **1**, 725-737.

HUYBRECHTS, P., LETREGUILLY, A., and REEH, N., 1991, The Greenland ice sheet and greenhouse warming. *Palaeography, Palaeoclimatology, Palaeoecology*, **89**, 399-412.

JOHNSEN, H., LAUKNES, L. and GUNERIUSSEN, T., 1995, Geocoding of fast-delivery ERS-1 SAR image mode product using DEM data. *International Journal of Remote Sensing*, **16**, 1957-1968.

JOUGHIN, I., 1995, *Estimation of ice-sheet topography and motion using interferometric synthetic aperture radar.* Ph.D. thesis, University of Washington.

JOUGHIN, I., WINEBRENNER, D., FAHNESTOCK, M., KWOK, R. and KRABILL, W., 1996, Measurement of ice-sheet topography using satellite-radar interferometry. *Journal of Glaciology*, **42**, 10-22.

KWOK, R., and FAHNESTOCK, M.A., 1996, Ice sheet motion and topography from radar interferometry. *I.E.E.E. Transactions on Geoscience and Remote Sensing*, **34**, 189-200.

PRESS, W.H., TEUKOLSKY, S.A., VETTERLING, W.T., and FLANNERY, B.P., 1992, *Numerical recipes in C: the art of scientific computing* (Cambridge: Cambridge University Press).

REES. W.G., and DOWDESWELL, J.A., 1988, Topographic effects on light scattering from snow. *Remote sensing: moving towards the 21st century, Proceedings of IGARSS '88 Symposium held in Edinburgh, Scotland, on 13-16 September 1988*, SP-284 (Paris: European Space Agency), pp. 161-164.

REES, W.G., 1992, Measurements of the fractal dimension of ice-sheet surfaces using Landsat data. *International Journal of Remote Sensing*, **13**, 663-671.

REES, W.G., 1995, Characterisation and imaging of fractal topography. *Fractals in Geoscience and Remote Sensing, Proceedings the JRC/EARSeL Expert Meeting held in Ispra, Italy, on 14-15 April 1994*, EUR 16092 EN (European Commission), pp. 298-324.

SMITH, W.H.F., and WESSEL, P., 1990, Gridding with continuous curvature splines in tension. *Geophysics*, **55**, 293-305.

STEPHENSON, S.N., and ZWALLY, H.J., 1989, Ice-shelf topography and structure determined using satellite radar altimetry and Landsat imagery. *Annals of Glaciology*, **12**, 162-169.

UNWIN, B.V., and WINGHAM, D.J., 1997, Topography and dynamics of Austfonna, Svalbard, from SAR interferometry. *Annals of Glaciology*, **24**, 403-408.

ZWALLY, H.J., BINDSCHADLER, R.A., BRENNER, A.C., MARTIN, T.V., and THOMAS, R.H., 1983, Surface elevation contours of Greenland and Antarctic ice sheets. *Journal of Geophysical Research*, **88**, 1589-1596.

Figures

Figure 1. Map of the Svalbard archipelago showing the main islands. The inset illustrates the position of Svalbard within the European Arctic sector.

Figure 2. Aircraft flight lines for radio echo sounding over Austfonna in spring 1983.

Figure 3. Grey-scaled Landsat MSS band 6 images of Austfonna projected onto UTM zone 35 coordinates. The images were acquired 25th March 1973 (top) and 1st August 1981 (bottom).

Figure 4. Scatterplots of Landsat MSS pixel brightness values and surface slope for (a) winter imagery and (b) summer imagery. There is a high correlation ($r^2 = 0.84$) between brightness values and surface slope in winter and no correlation during summer.

Figure 5. Surface elevation along a profile passing across the centre of Austfonna and parallel to the solar azimuth. RES tie-points are represented by circles, interpolated surface elevation calculated by a minimal squared curvature function is represented by the dotted line and shape-from-shading derived surface elevation is represented by the solid line. Deviation of the shape-from-shading profile from the RES tie-points is a product of the inversion algorithm and is occasionally greater than 20 m.

Figure 6. DEM of Austfonna derived from RES data gridded using shape-from-shading.

Figure 7. Fourier transform of the errors in the shape-from-shading DEM.

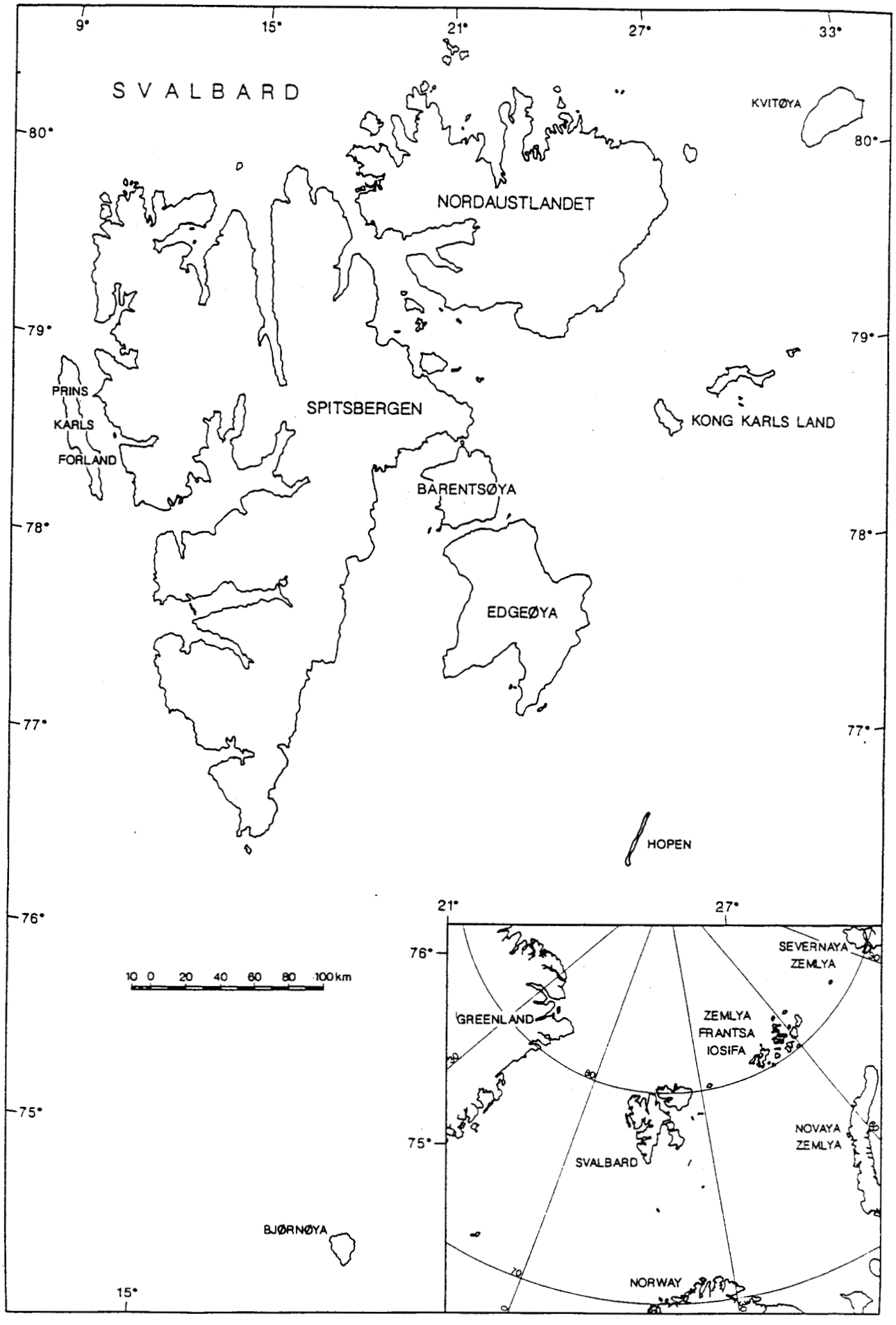
SVALBARD
KVITØYA
NORDAUSTLANDET
SPITSBERGEN
PRINS
KARLS
FORLAND
KONG KARLS LAND
BARENTSØYA
EDGEØYA
HOPEN
BJØRNØYA
9°
15°
21°
27°
33°
80°
79°
78°
77°
76°
75°
10 0 20 40 60 80 100 km
GREENLAND
SEVERNAYA ZEMLYA
ZEMLYA FRANTSA IOSIFA
SVALBARD
NOVAYA ZEMLYA
NORWAY

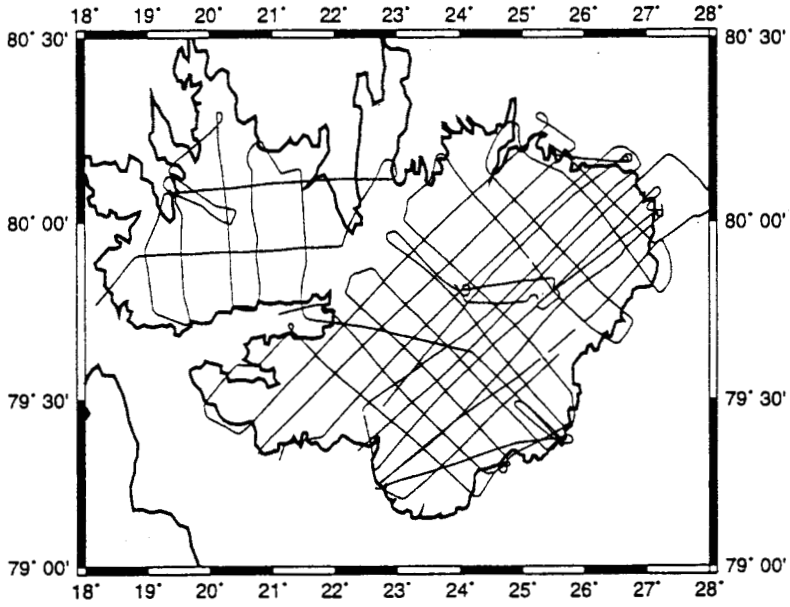

Figure 2:

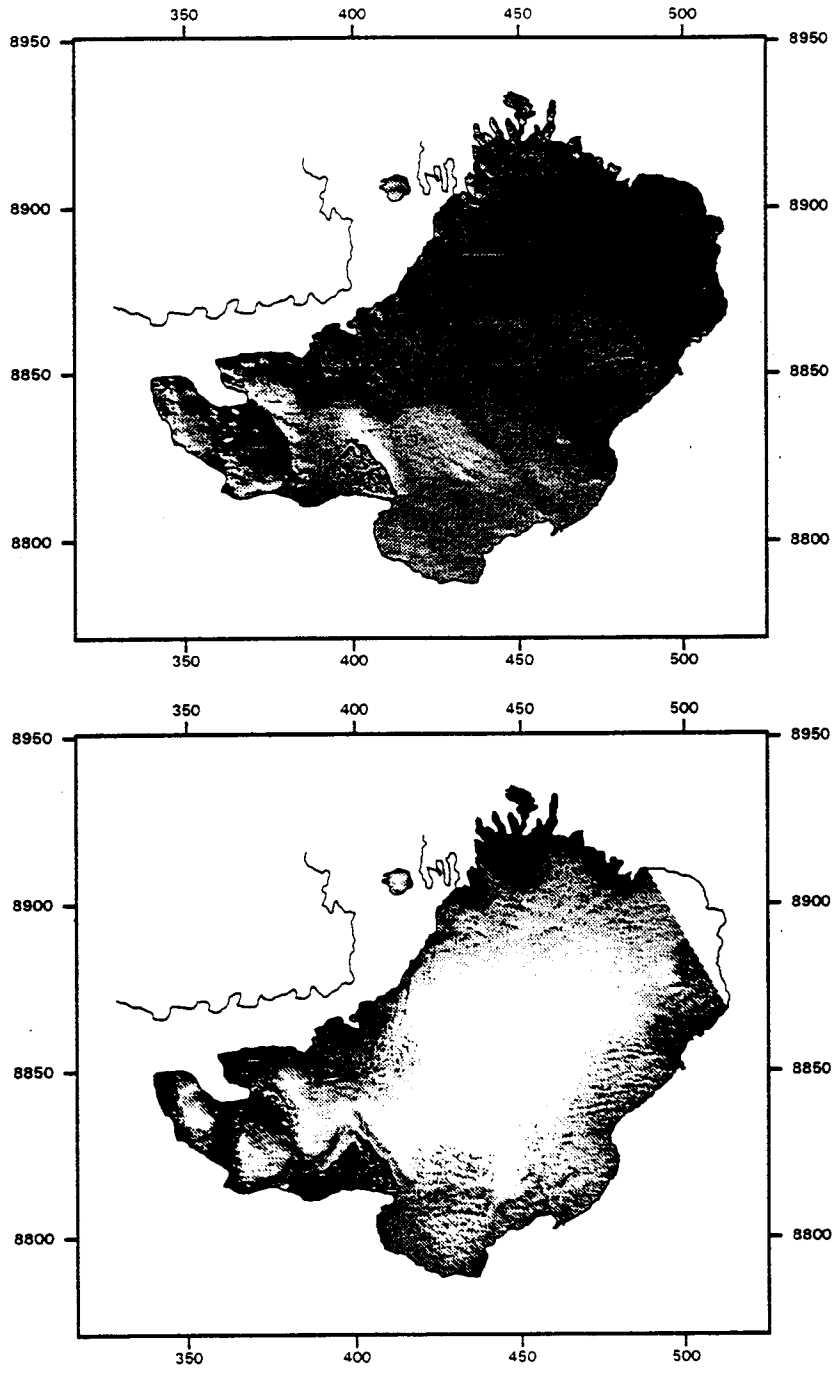

Figure 3:

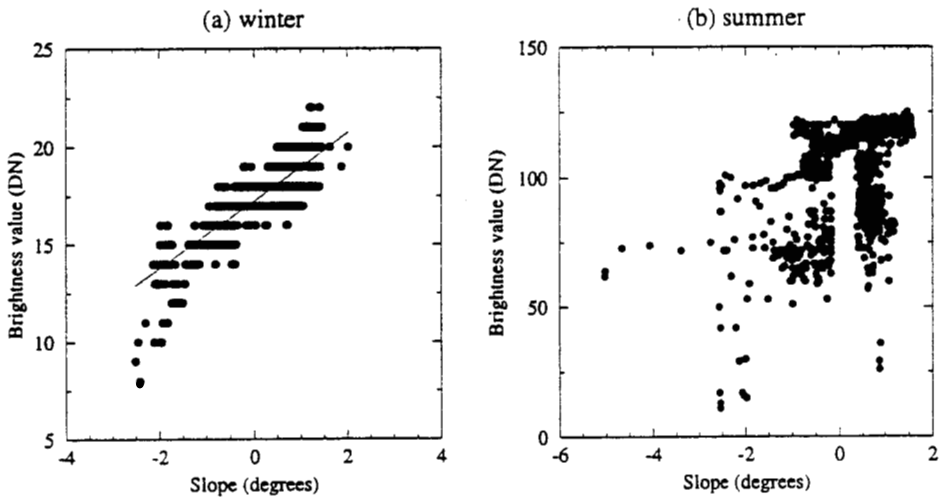
(a) winter
(b) summer
Brightness value (DN)
Slope (degrees)
25
20
15
10
5
-4
-2
0
2
4
150
100
50
0
-6

Figure 4:

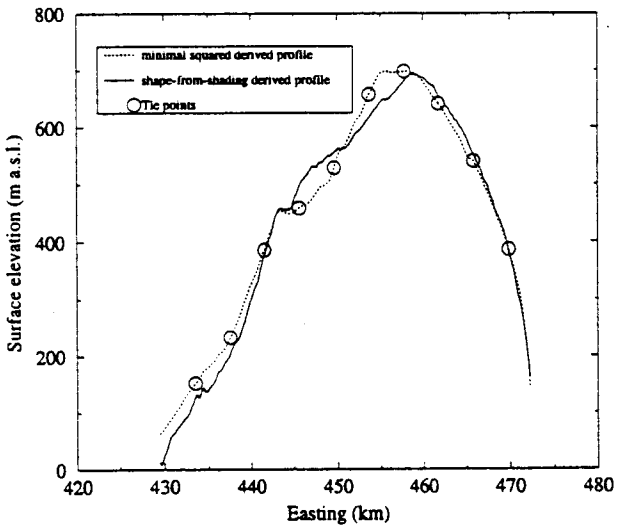
minimal squared derived profile
shape-from-shading derived profile
Tie points
Surface elevation (m a.s.l.)
Easting (km)
800
600
400
200
0
420
430
440
450
460
470
480

Figure 5:

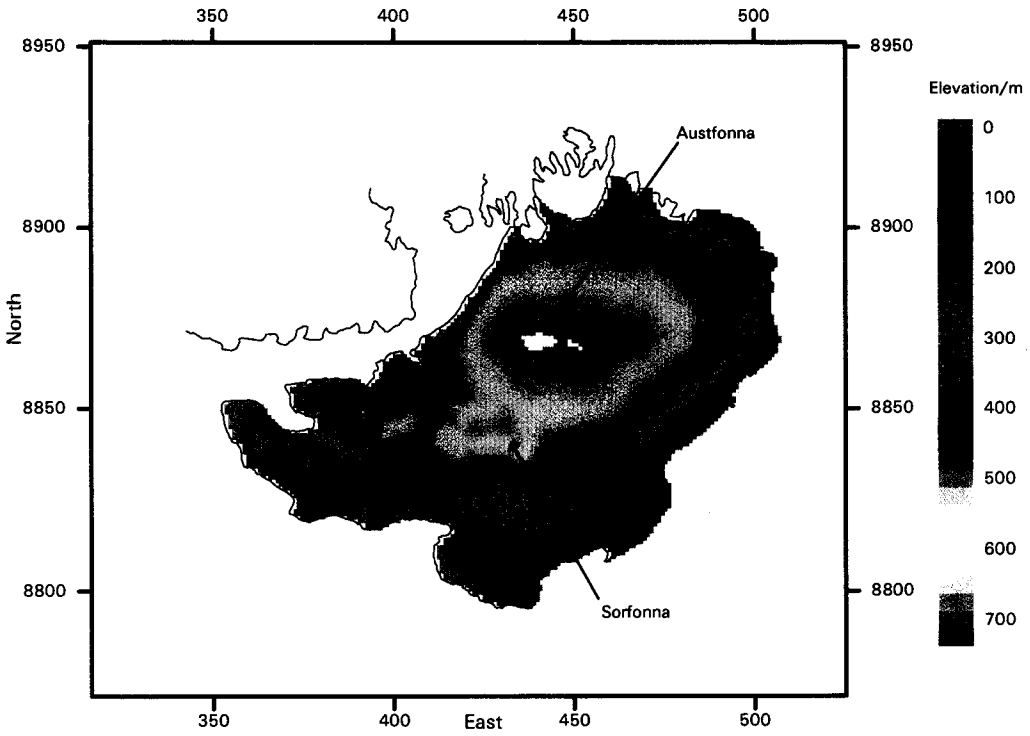
350
400
450
500
8950
8900
8850
8800
North
East
Austfonna
Sorfonna
Elevation/m
0
100
200
300
400
500
600
700

Figure 6:

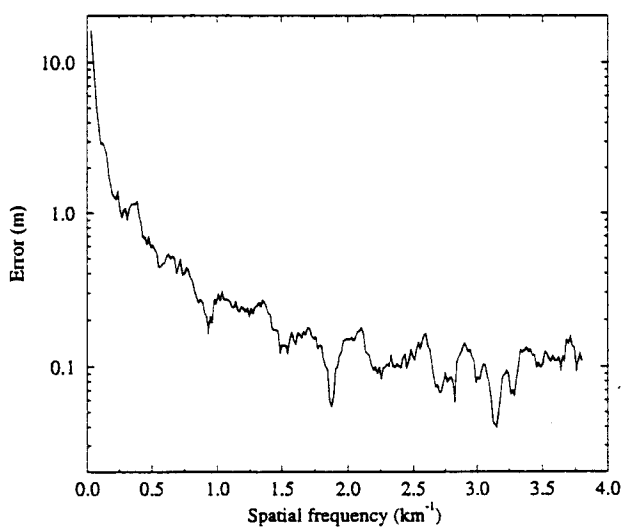
10.0
1.0
0.1
Error (m)
0.0
0.5
1.0
1.5
2.0
2.5
3.0
3.5
4.0
Spatial frequency (km-1)

Figure 7: